Thermoforming Process of Amorphous Polymeric Sheets: Modeling and Finite Element Simulations

A. Makradi,[1] S. Belouettar,[2] S. Ahzi,[1] S. Puissant[3]

[1]*Institut de Mécanique des fluides et des Solides, University Louis Pasteur, UMR 7507, 2 Rue Boussingault, 67000 Strasbourg, France*
[2]*LTI, Research Center Henry Tudor, 70 Rue de Luxembourg, L-4221 Esch-sur-Alzette, Luxembourg, France*
[3]*Institut Supérieur d'Ingénierie de Conception, Equipe de Recherche en Mécanique et Plastique, 27 Rue d'Hellieule, 88100 St Dié-des-Vosges, France*

Received 23 October 2006; accepted 27 April 2007
DOI 10.1002/app.26869
Published online 17 July 2007 in Wiley InterScience (www.interscience.wiley.com).

ABSTRACT: A temperature and strain rate dependent model for the thermoforming process of amorphous polymer materials is proposed. The polymeric sheet is heated at a temperature above the glass transition temperature then deformed to take the mold shape by the means of an applied pressure. The applied process temperature is taken uniform throughout the sheet and its variation is due only to the adiabatic heating. The behavior of the polymeric material is described by a micromechanically-based elastic-viscoplastic model. The simulations are conducted for the poly(methyl methacrylate) using the finite element method. The polymer sheet thickness and the orientation of the polymer molecular chains show an important dependence on the process temperature, the applied pressure profile, and the contact forces with the mold surface. © 2007 Wiley Periodicals, Inc. J Appl Polym Sci 106: 1718–1724, 2007

Key words: polymer thermoforming; micromechanical model; poly(methyl methacrylate); finite element method

INTRODUCTION

The thermoforming process of thermoplastic polymeric materials consists of heating and subsequently deforming into the mold of a thin plastic sheet at a temperature above its glass transition temperature. A simplified schematic diagram of the pressure thermoforming process is reported in Figure 1. The thin plastic sheet, clamped at the edges, is heated to a softened state by means of a radiative heat transfer. Then immediately after the heater is removed, the plastic sheet is deformed to take the mold shape by an applied pressure. The pressure is applied either to the upper face of the plastic sheet or by the evacuation of the air between the plastic sheet and the mold. Before removing the applied pressure, the freezing step take place by cooling the polymer to a temperature below its glass transition to conserve the desired final product geometry and its molecular structure developed during the hot deformation stage. The behavior of polymeric materials in this process is strongly affected by the stress level, the rate of loading and the test temperature.[1] Therefore, an appropriate control of the process strain rate and temperature, leads to better control of the thermally activated micromechanical processes in these materials during the thermoforming process.

Work on the thermoforming of polymeric materials is reported recently by Aus Der Wiesche[2] considering a viscoelastic constitutive model. Warby et al.[3] considered a constitutive model independent on the temperature and on the strain rate, where the parameters are calibrated on an experimental stress–strain curve at constant temperature and strain rate. Schmidt et al.[4] developed a 3D numerical method and an experimental set up to simulate and measure the plastic sheet temperature during the heating stage.

The present article focuses on a micromechanically-based elastic-viscoplastic modeling and the simulation of the thermoforming process of amorphous polymers. The model considers the dependence on temperature and strain rate in relating the macroscopic response to the micromechanical processes. In the present work the process temperature is assumed constant and uniform, but the variation of the plastic sheet temperature may arise from the adiabatic heating. The proposed micromechanical model is implemented in the commercial finite element software Abaqus[5] via a user material subroutine material.

CONSTITUTIVE MODEL

The following notations are used: $\boldsymbol{F}$ deformation gradient tensor; $\boldsymbol{V}$ stretch tensor; $\boldsymbol{R}$ rotation tensor; $\boldsymbol{L}$ velocity gradient tensor; $\boldsymbol{D}$ strain rate tensor; $\boldsymbol{W}$ spin

Correspondence to: A. Makradi (makradi@imfs.u-strasbg.fr).
Contract grant sponsor: Luxembourgish National Research Fund (to A. M.); contract grant number: FNR (MA6/06/16).

Journal of Applied Polymer Science, Vol. 106, 1718–1724 (2007)

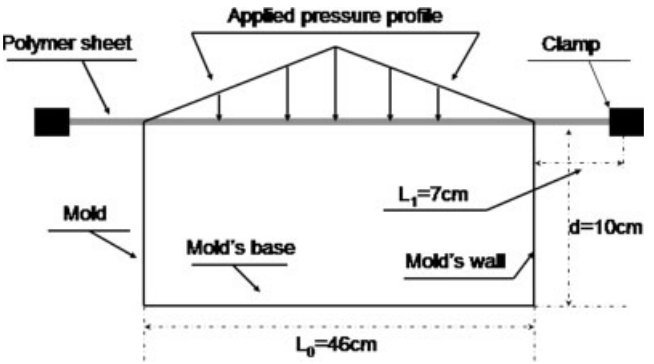

Figure 1 Schematic diagram of pressure thermoforming process.

tensor; $\boldsymbol{T}$ Cauchy stress tensor; θ absolute temperature; τ effective shear stress.

The three-dimensional constitutive model used to describe the large deformation behavior is based on the work of Boyce et al.[6] and that of Makradi et al.[7,8] The analog representation considers an intermolecular resistance (resistance A) acting in parallel with a network resistance (resistance B) (see Fig. 2). The total imposed deformation gradient $\boldsymbol{F}$ is identical to both the intermolecular, $\boldsymbol{F}_A$, and the network deformation gradients, $\boldsymbol{F}_B$:

$$\boldsymbol{F} = \boldsymbol{F}_A = \boldsymbol{F}_B \tag{1}$$

Therefore, the total Cauchy stress $\boldsymbol{T}$ is the sum of the intermolecular Cauchy stress, $\boldsymbol{T}_A$, and the network Cauchy stress, $\boldsymbol{T}_B$:

$$\boldsymbol{T} = \boldsymbol{T}_A = \boldsymbol{T}_B \tag{2}$$

Intermolecular resistance: Resistance A

The intermolecular behavior consists of an initially stiff response followed by a flow. This behavior is represented in the analog model as a spring in series with a viscous element. The deformation can therefore be decomposed into elastic $\boldsymbol{F}_A^{\mathrm{e}}$ and thermoplastic $\boldsymbol{F}_A^{\mathrm{thp}}$ components via the multiplicative decomposition of the intermolecular resistance deformation gradient, $\boldsymbol{F}_A$:

$$\boldsymbol{F}_A = \boldsymbol{F}_A^{\mathrm{e}}\boldsymbol{F}_A^{\mathrm{thp}} \quad \text{with} \quad \boldsymbol{F}_A^{\mathrm{e}} = \boldsymbol{V}_A^{\mathrm{e}}\boldsymbol{R}_A^{\mathrm{e}} \tag{3}$$

Here $\boldsymbol{V}_A^{\mathrm{e}}$ is the elastic stretch tensor and $\boldsymbol{R}_A^{\mathrm{e}}$ is the elastic rotation tensor.

Equation of stress

The Cauchy stress is given by the following relation:

$$\boldsymbol{T}_A = \frac{1}{J_A}\Im^{\mathrm{e}}\left[\ln\left(\boldsymbol{V}_A^{\mathrm{e}}\right)\right] \tag{4}$$

where $J_A = \det(\boldsymbol{F}_A^{\mathrm{e}})$ is the volume change, $\Im^{\mathrm{e}}$ is the fourth order elastic stiffness tensor, and $\ln(\boldsymbol{V}_A^{\mathrm{e}})$ is the Hencky strain.

Evolution equation for $\boldsymbol{F}_A^{\mathrm{thp}}$: Flow rule

Using the definition of the velocity gradient we can write:

$$\dot{\boldsymbol{F}}_A^{\mathrm{thp}} = \boldsymbol{L}_A^{\mathrm{thp}}\boldsymbol{F}_A^{\mathrm{thp}}$$
$$\text{with} \begin{cases} \boldsymbol{L}_A^{\mathrm{thp}} = \boldsymbol{W}_A^{\mathrm{thp}} + \boldsymbol{D}_A^{\mathrm{thp}} \\ \boldsymbol{W}_A^{\mathrm{thp}} = 0; \quad \boldsymbol{D}_A^{\mathrm{thp}} = \boldsymbol{D}^{\mathrm{p}} + \beta(\theta)\dot{\theta}\cdot\boldsymbol{I} \\ \boldsymbol{D}^{\mathrm{p}} = \dfrac{\dot{\gamma}_A}{\sqrt{2}\tau_A}\dot{\boldsymbol{T}}'_A, \quad \tau_A = \left(\dfrac{1}{2}\boldsymbol{T}'\cdot\boldsymbol{T}'\right)^{1/2} \end{cases} \tag{5}$$

Here β(θ) is the temperature dependent linear thermal expansion coefficient. The rate of the viscous flow, $\dot{\gamma}_A$, follow the Arhenius type expression proposed by Argon[1] and modified by Boyce et al.[6,9]

$$\dot{\gamma}_A = \dot{\gamma}_o \exp\left[\frac{A\cdot(s+\alpha\cdot p)}{\theta}\left(1-\frac{\tau_A}{s+\alpha\cdot p}\right)\right] \tag{6}$$

The parameters $\dot{\gamma}_o$ and s are, respectively, the reference shear rate and the deformation resistance. The parameters A, s, and $\dot{\gamma}_o$ are, fitting parameters (Table I), chosen to reproduce the experimental dependence on temperature and strain rate of stress–strain response.[1] We note that there exist other models in the literature, which may describe the behavior in a better way, particularly for temperature above T_g and on a wide range of strain rates.[10,11] However, for simplicity we use the modified Argon's model, which shows fairly good results to moderate strain rates.[6–8]

Network stress and flow: Resistance B

The deformation acting on the network resistance represents the network orientation process and the molecular relaxation process. The deformation gradient $\boldsymbol{F}_B$ can be decomposed into a network orientation

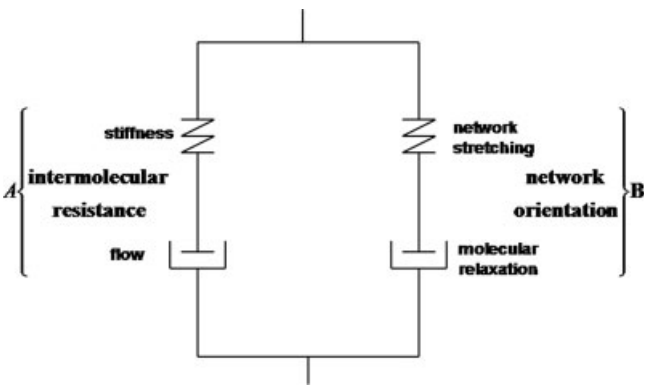

Figure 2 Schematic representation of the breakdown of the total resistance into an intermolecular resistance and network resistance.

TABLE I
Physical and the Model Parameters

Parameter	Equation	Value
$\dot{\gamma}_o$	(6)	1.75×10^5
s (MPa)	(6)	56
A (K^{-1})	(6)	126.85
α	(6)	0.26
C_R (0) (MPa)	(9)	85.42
a	(9)	0.2106
N_{rl} (0)	(9)	0.2
b	(9)	0.0012
T_g^{ref}	(10)	387
c_1	(10)	32.58
c_2	(10)	83.5
$\dot{\varepsilon}_{ref}$	(10)	1
C_F (MPa × s)$^{-1}$	(12)	0.6×10^3
ρ (298 K)	(19)	1337
c_p (298 K)	(20)	1835
Young Modulus E (MPa)	(4)	200
Poisson ratio ν	(4)	0.43

part $\boldsymbol{F}_B^n$ and a flow part $\boldsymbol{F}_B^f$. The multiplicative decomposition is given as:

$$\boldsymbol{F}_B = \boldsymbol{F}_B^n \boldsymbol{F}_B^f \tag{7}$$

Equation of stress

The network stress is described by the Arruda and Boyce's[12] eight chains model, where a stress-stretch relation is formulated as follows:

$$\boldsymbol{T}_B = \frac{1}{J_B} C_R \frac{\sqrt{N_{rl}}}{\bar{\lambda}_n} \ell^{-1}\left(\frac{\bar{\lambda}_n}{\sqrt{N_{rl}}}\right)\left[\bar{\boldsymbol{B}}^n - (\bar{\lambda}_n)^2 \boldsymbol{I}\right] \tag{8}$$

Here $J_B = \det(\boldsymbol{F}_B^n)$ is the network volume change, ℓ^{-1} is the inverse Langevin function given by the Padé approximation $\ell^{-1}(x) \approx x(3 - x^2)/(1 - x^2)$. The number of rigid links between entanglement N_{nl} and the rubbery modulus C_R, function of the glace transition temperature T_g, are described by the following phenomenological equation proposed by Richeton et al.[10]

$$\begin{aligned} C_R(\theta \geq T_g) &= \frac{C_R(0) - a \cdot T_g}{T_g} \cdot \theta \\ N_{rl}(\theta \geq T_g) &= N_{rl}(0) + b \cdot T_g \end{aligned} \tag{9}$$

$$\text{with} \quad T_g = T_g^{ref} + \frac{-c_2 \cdot \log\left(\dot{\varepsilon}^{ref}/\dot{\varepsilon}\right)}{c_1 + \log\left(\dot{\varepsilon}^{ref}/\dot{\varepsilon}\right)} \tag{10}$$

where $C_R(0)$, a, $N(0)$, b are material parameters and c_1, c_2 are the Williams, Landel, and Ferry[13] (WLF) parameters relative to the reference glass transition temperature T_g^{ref} (Table I).

The stretch on each chain in the network, $\bar{\lambda}_n$, [eq. (8)] is the root mean square of the distortional applied network stretches:

$$\bar{\lambda}_n = \left[\left(1/3\right) tr\left(\bar{\boldsymbol{B}}^n\right)\right]^{1/2} \tag{11}$$

where $\bar{\boldsymbol{B}}^n = \bar{\boldsymbol{F}}_B^n \, (\bar{\boldsymbol{F}}_B^n)^T$ and $\bar{\boldsymbol{F}}_B^n = (J_B)^{-1/3} \, \boldsymbol{F}_B^n$

Evolution equation for F_B^f: Flow rule

Using the velocity gradient $\mathbf{L}_B^f$ we can write:

$$\dot{\boldsymbol{F}}_B^f = \boldsymbol{L}_B^f \boldsymbol{F}_B^f \quad \text{with} \quad \begin{cases} \boldsymbol{L}_B^f = \boldsymbol{W}_B^f + \boldsymbol{D}_B^f \\ \boldsymbol{W}_B^f = 0; \quad \boldsymbol{D}_B^f = \dfrac{\dot{\gamma}_B^f}{\sqrt{2}\tau_B} \boldsymbol{T}'_B \end{cases} \tag{12}$$

The relaxation process is prescribed by Bergstrom and Boyce's model[14] via the stress-assisted chain reptation based on Doi and Edwards[15] theory. The rate of relaxation is taken to be:

$$\dot{\gamma}_B^f = C_F\left(\frac{1}{\lambda_f - 1}\right)\tau_B \tag{13}$$

where $\lambda_f = \lfloor 1/3(tr(\boldsymbol{F}_B^f(\boldsymbol{F}_B^f)^T)) \rfloor$, $\tau_B = (1/2(\boldsymbol{T}'_B \cdot \boldsymbol{T}'_B)^{1/2})$, and C_F is a parameter that expresses the temperature dependence.

Adiabatic heatings

The basic differential energy balance equation is given by:

$$\rho(\theta) \cdot C_p(\theta) \cdot \dot{\theta} - \mathrm{div}(\Gamma(\theta) \cdot \mathrm{grad}(\theta)) = \dot{q} \tag{14}$$

where $\rho(\theta)$ is the density, $C_p(\theta)$ is the specific heat, $\Gamma(\theta)$ is the thermal conductivity, and $\dot{q}$ is the rate of heat generation due only to plastic flow[16] and is equal to [Trace($\boldsymbol{T}'\boldsymbol{D}^p$)]. The plastic work associated with the back stress is supposed to be stored as free energy in the material because of locked-in orientation.[17] In our simulation, the thermal conductivity term is neglected and the quantity [trace($\boldsymbol{T}'\boldsymbol{D}^p$)] is approximated by $[\tau_A \cdot \dot{\gamma}^p]$. The resulting energy balance equation is then given by:

$$\dot{\theta} = \frac{\tau_A \cdot \dot{\gamma}^p}{\rho(\theta) \cdot c(\theta)} \tag{15}$$

TIME UPDATING AND INTEGRATION PROCEDURE

The proposed elastic–viscoplastic constitutive model describing the large deformation of an amorphous

polymer above its glass transition temperature is implemented into the commercial finite element code Abaqus[5] explicit via the user material subroutine VUMAT. This section focuses on the algorithm's structure and the numerical time integration within each time step.

To calculate the total Cauchy Stress $\boldsymbol{T} = \boldsymbol{T}_A + \boldsymbol{T}_B$ from eqs. (4) and (8) at time: $(t + \Delta t)$, we need to calculate respectively the elastic deformation gradient $\boldsymbol{F}_A^{\mathrm{e}}$ and the orientation deformation gradient $\boldsymbol{F}_B^{\mathrm{n}}$.

$$\left(\boldsymbol{F}_A^{\mathrm{e}} = \boldsymbol{F}\left(\boldsymbol{F}_A^{\mathrm{thp}}\right)^{-1}\right)^{t+\Delta t} \quad \text{and} \quad \left(\boldsymbol{F}_B^{\mathrm{n}} = \boldsymbol{F}\left(\boldsymbol{F}_B^{\mathrm{f}}\right)^{-1}\right)^{t+\Delta t} \tag{16}$$

where the total deformation $\boldsymbol{F}$ is calculated from the guess value displacement at each time step. If the local developed total Cauchy stress $\boldsymbol{T}$ is not enough to reach the yield stress, there is no viscoplastic deformation, $\boldsymbol{F}_A^{\mathrm{thp}} = \boldsymbol{I}$ and $\boldsymbol{F}_B^{\mathrm{f}} = \boldsymbol{I}$. The contribution to the total Cauchy stress of the molecular orientation $\boldsymbol{T}_B$ is neglected prior to the yielding. Once the local Cauchy stress reaches the yield stress, $\boldsymbol{F}_A^{\mathrm{thp}}$ and $\boldsymbol{F}_B^{\mathrm{f}}$ deviate from the unit tensors and they have to be derived from the viscoplastic flow rules, eqs. (5), (6), and (12), (13), respectively. Expressions for the change in plastic deformation gradient $\dot{\boldsymbol{F}}_{t+\Delta t}^{\mathrm{p}}\,\Delta t$ and the change in flow deformation gradient $\dot{\boldsymbol{F}}_{t+\Delta t}^{\mathrm{f}}\,\Delta t$ are found in the beginning, respectively, with the definitions of the plastic velocity gradient $\dot{\boldsymbol{F}}_A^{\mathrm{thp}} = \boldsymbol{D}_A^{\mathrm{thp}}\,\boldsymbol{F}_A^{\mathrm{thp}}$ and flow velocity gradient $\dot{\boldsymbol{F}}_B^{\mathrm{f}} = \boldsymbol{D}_B^{\mathrm{f}}\,\boldsymbol{F}_B^{\mathrm{f}}$. The equations to update $(\boldsymbol{F}_A^{\mathrm{thp}})_{t+\Delta t}$ and $(\boldsymbol{F}_B^{\mathrm{f}})_{t+\Delta t}$ are given by:

$$\begin{aligned}\left(\boldsymbol{F}_A^{\mathrm{thp}}\right)_{t+\Delta t} &= \left(\boldsymbol{F}_A^{\mathrm{thp}}\right)_t + \left(\boldsymbol{D}_A^{\mathrm{thp}}\boldsymbol{F}_A^{\mathrm{thp}}\right)_{t+\Delta t}\Delta t \quad \text{and} \\ \left(\boldsymbol{F}_B^{\mathrm{f}}\right)_{t+\Delta t} &= \left(\boldsymbol{F}_B^{\mathrm{f}}\right)_t + (\boldsymbol{D}_B^{\mathrm{f}}\boldsymbol{F}_B^{\mathrm{f}})_{t+\Delta t}\,\Delta t\end{aligned} \tag{17}$$

At each time step, the temperature $\theta_{t+\Delta t}$ is updated using the backward difference algorithm:

$$\theta_{t+\Delta \mathrm{t}} = \theta_t + \dot{\theta}\cdot\Delta t \tag{18}$$

where the temperature time rate $\dot{\theta}$ is calculated from the eq. (15).

The contact between the mold surface and the polymer sheet is described by the Coulomb's friction model,[5] where the friction coefficient μ is taken equal to 0.15.

MATERIAL PROPERTIES

To verify the model described earlier, we chose the poly(methyl methacrylate) (PMMA) because the experimental data needed for the calibration of the constitutive equation could be found in the literature.[18] The dependence on temperature and strain rate of the PMMA material properties can be found in the work of Richeton et al.[10] Above the glass transition temperature the physical properties of polymers are known to be strongly influenced by temperature and in particular by the glass transition temperature, T_g. Empirical and semi-empirical formulae can be found in the books of van Krevelen[19] and Bicerano,[20] to determine the temperature dependence of material properties as a function of its corresponding values at temperature $\theta = 298$ K. The temperature dependence of the density, $\rho(\theta)$, and the heat capacity, $c_p(\theta)$, are given by[10]:

$$\rho\left(\theta \geq T_g\right) = \rho(298\mathrm{K})\cdot\frac{(1.42T_g + 44.7)}{1.27T_g + 0.30\cdot\theta} \tag{19}$$

$$c_p(\theta \geq T_g) = c_p(298\mathrm{K})\cdot(0.613 + 1.3\cdot10^{-3}\cdot\theta) \tag{20}$$

where the parameters $\rho(298\ \mathrm{K})$ and $c_p(298\ \mathrm{K})$ are, respectively, the density and the heat capacity of the PMMA at temperature $\theta = 298$ K.

All the parameters required for eqs. (19) and (20) are given in Table I.

RESULT AND DISCUSSION

The mold considered for the thermoforming process simulations is circular with a total diameter $\ell = 0.6$ m and a depth $d = 0.1$ m (see Fig. 1). To determine the model parameters of the PMMA material, the predicted true stress-true strain response is compared to experimental data[18] (see Fig. 3) for an uniaxial compression test performed at a temperature, = 115°C, and at a constant nominal strain rate, $\dot{\varepsilon} = 0.0067\mathrm{s}^{-1}$. The true stress-true strain curves (Fig. 3)

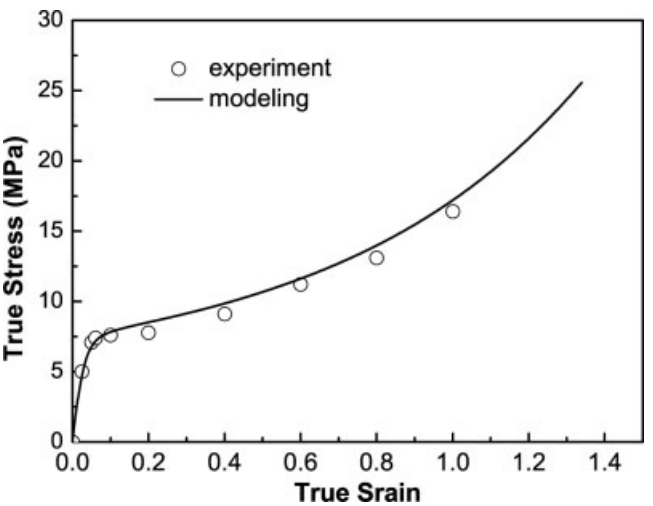

Figure 3 A compression stress-strain response at nominal strain rate of $\dot{\varepsilon} = 0.0067\ \mathrm{s}^{-1}$ in comparison with the experimental data[18] at 115°C.

exhibits the four characteristic regions of polymeric material above the glass transition temperature. Under small deformation the material show a relatively stiff modulus, followed by a rollover to flow at 7.5 MPa. At moderate deformation, the material shows gradual stiffening followed by a dramatic hardening at large deformation. The physical and the model parameters are summarized in Table I. It should be noted that the simulated results on Figure 3 are conducted under constant ''true'' strain rate tests. The comparison with the experimental results of Doolong et al.[18] may not be very adequate since these results are obtained by loading under constant ''nominal'' strain rate.

To verify the model, the predicted thickness distribution of Acrylic (PMMA) sheet is compared with the experimental results of Dong et al.[21,22] and good agreement is found (see Figs. 4 and 5). The experiment consists of applying a pressure of 20 kPa and 40 kPa on a rectangular polymeric sheet (29 cm long $\times$ 10 cm wide) (bubble inflation test) at temperature $\theta = 160^{\circ}C$. Figures 4 and 5 present the relative sheet thickness in the hoop direction and longitudinal direction respectively versus the deformed length of the sheet. The sheet used for this thermoforming test has a thickness of 0.3 cm and a density $\rho = 1200$ kg/m^3, whereas the model parameters used in these simulations are kept the same as the ones used to fit the true stress–stain uniaxial compression (Table I).

To illustrate the effect of the mold on the polymeric sheet during the thermoforming test a disc mold with a diameter of 0.6 m is used. A part of this sheet is shown in Figure 6 at the deformed shape. The time evolution of the applied pressure during the thermoforming process depends on the degree of the complexity of mold geometry. This makes the boundary condition corresponding to the applied

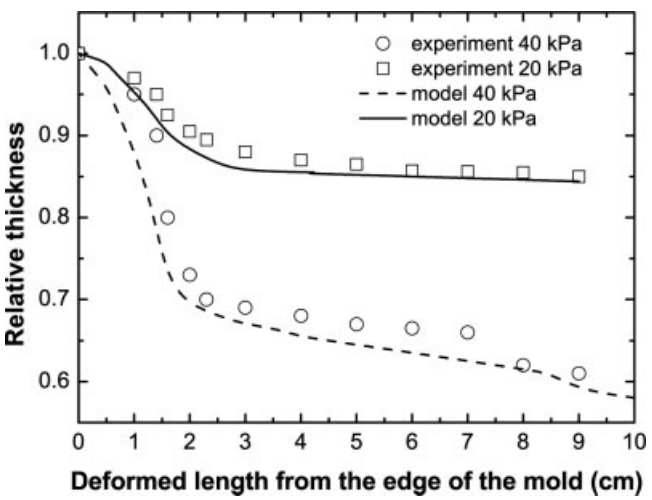

Figure 4 Predicted thickness of the Acrylic (PMMA) sheet in the hoop direction at the middle of the sheet compared to the experimental data[21,22] at 160°C.

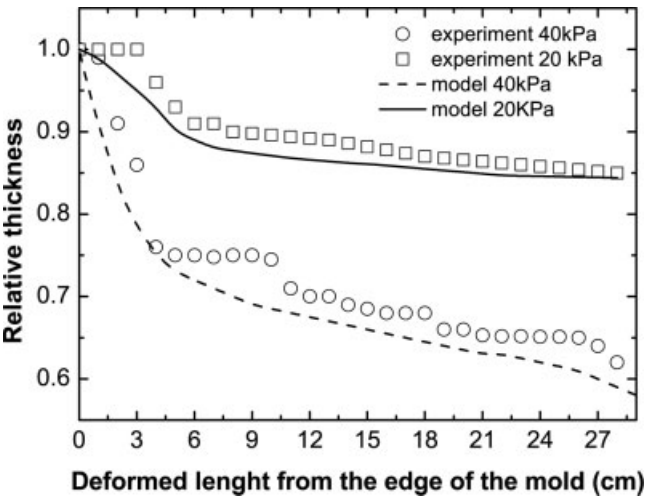

Figure 5 Predicted thickness of the Acrylic (PMMA) sheet in the longitudinal direction at the middle of the sheet compared to the experimental data[21,22] at 160°C.

pressure difficult to set. In our simulation the applied pressure is chosen to be time independent, linear between the center and the wall of the mold (Fig. 1). The maximal applied pressure is on the center of the mold ($P = 20$ MPa) then decreases linearly to vanish on the wall of the mold. Between the clamp and the wall the sheet lays on the mold surface and the applied pressure on this surface is zero. The only variation of the sheet thickness in this region stems from the stretching due to the applied

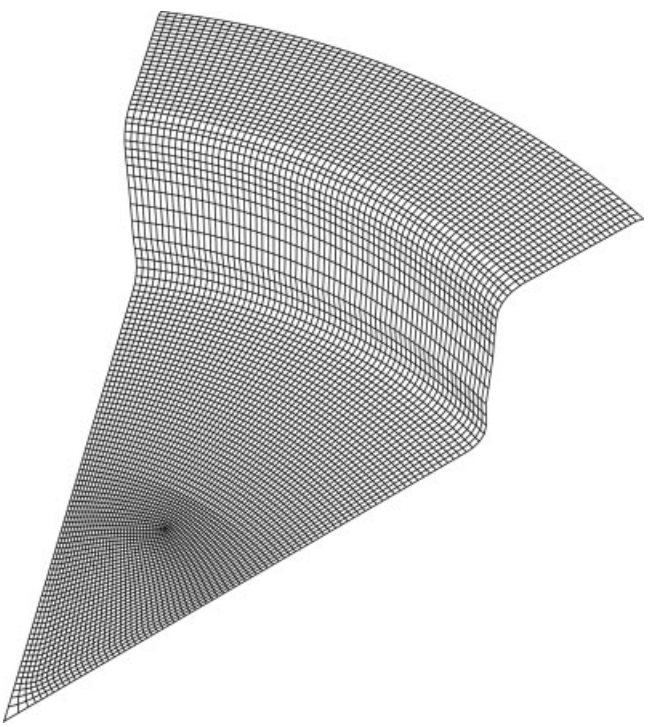

Figure 6 Deformed shape of the polymeric sheet: Mesh distribution.

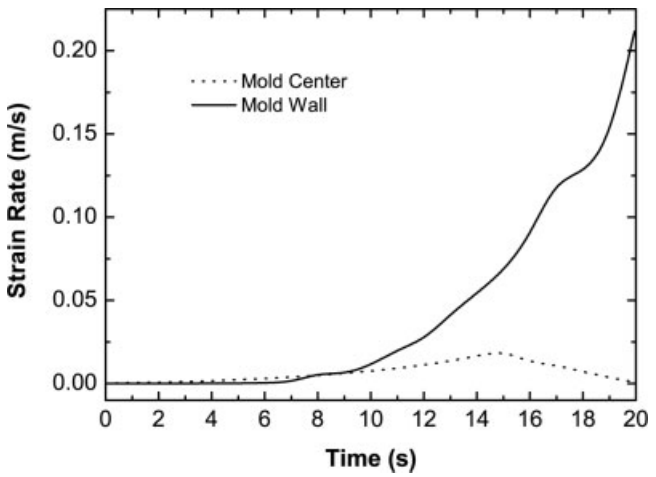

Figure 7 Strain rate time dependence of the polymer sheet on the wall and the center of the mold.

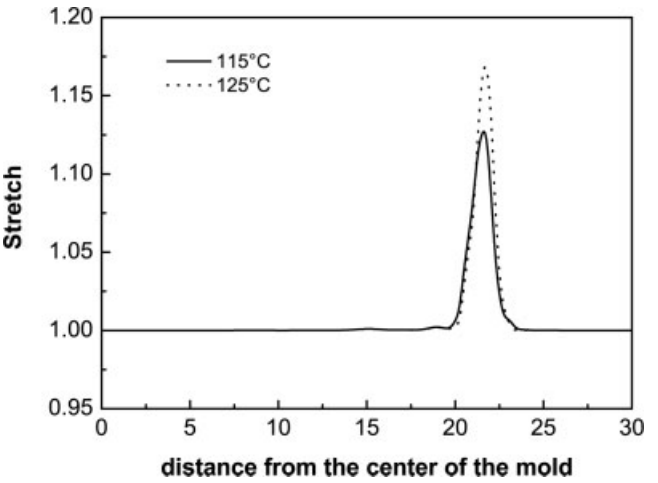

Figure 9 Predicted profile of the polymer molecular chains equivalent stretch for different temperature from the center of the mold to the clamp.

pressure inside the mold. Figure 7 illustrate the time dependence of the strain rate on the wall and the center of the mold. This behavior is due the material's dependence on time which is expressed by eq. (6). The temperature dependence of the sheet thickness which is the main parameter to control during the thermoforming process is reported in Figure 8. The sheet thickness depends strongly on the radial applied pressure profile. Once the pressure is applied, the radial sheet thickness profile shows a minimum on the center of the mold and a maximum between the wall and the clamp, due to the radial distribution of the applied pressure. However, once the sheet gets in contact with the mold's surface, a surface contact force rises which prevent the sheet to stretch freely. Since the contact of the sheet and the mold's surface starts at the mold's center and spreads till the mold's wall, the effects of the contact force and the applied pressure result in a nonlinear decrease of the sheet thickness towards the mold's wall. At the edge between the mold's base and the mold's wall the applied pressure pushes the soft polymer to the edge, which results in a stabilization and a slight increase of the sheet thickness in this region. On the mold's wall, the thickness of the sheet shows a dramatic decrease because it's the last part of the sheet to get in contact with the mold's surface. On the mold's wall surface, the sheet stretches freely under the applied pressure without any contact with the mold's surfaces. This large variation of the sheet thickness on the mold's wall surface induces an important orientation of the polymer molecular chains (see Fig. 9). Figure 9 shows the equivalent molecular chains stretch, $\bar{\lambda}_n$, calculated from eq. (11). The

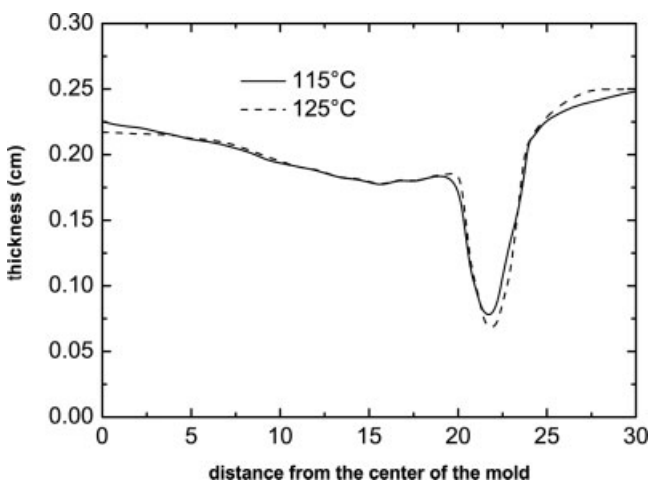

Figure 8 Predicted profile of the polymeric sheet thickness for different temperatures from the center of the mold to the clamp.

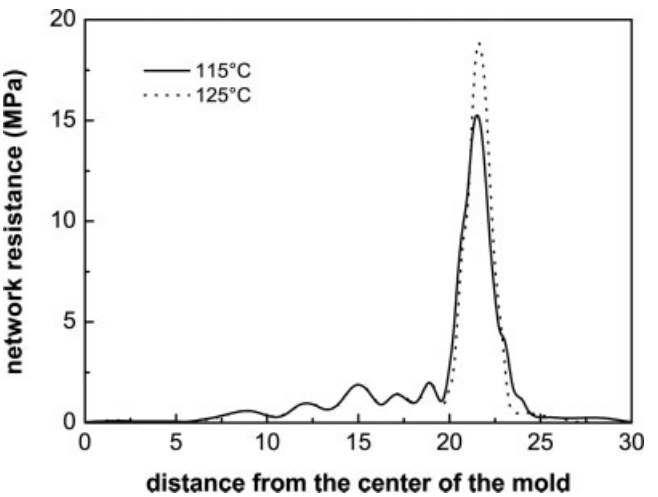

Figure 10 Predicted profile of the polymer molecular chains equivalent stretch for different temperature from the center of the mold to the clamp.

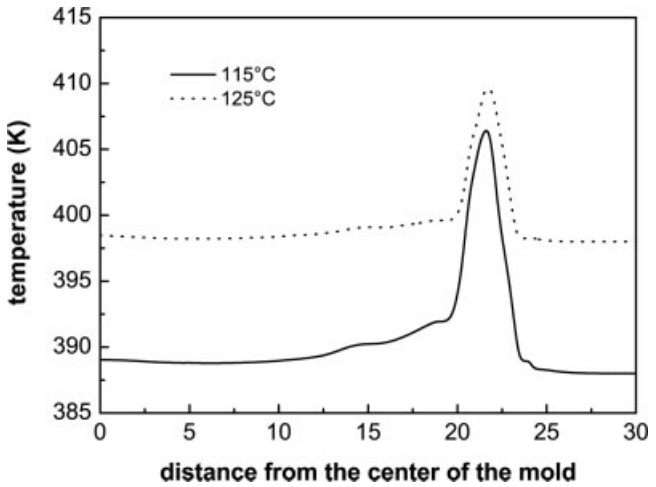

Figure 11 Sheet temperature profile for different temperature tests from the mold's center to the clamp.

increase of temperature results in a slight reduction of the sheet thickness on the mold's wall, which in turn results on a significant increase of the polymer molecular chains orientation in this region. This temperature dependence of the molecular orientation might not be as important as it is seen in Figure 10. In fact, we did not account of the dependence on temperature of the chains relaxation's rate through the parameter C_F [eq. (13)] as it is suggested by Boyce et al.[6] The high molecular orientation induces an important contribution of the network resistance [eq. (8)] to the mechanical properties of the final product. Figure 10 shows the equivalent Mises network resistance

$$(T_B)_{\text{eq}} = \sqrt{(3/2)(T_B)_{ij}(T_B)_{ij}}$$

profile, which is maximum on the mold's wall region because of high orientation of the polymer molecular chains in this region. The variation of the network resistance between the mold's center and mold's wall is due to the contact of the polymer sheet with the mold's base surface. The radial polymer sheet temperature profile is shown in Figure 11 for the two test temperatures used in our simulations. The temperature curves show a slight variation between the mold's center and the molds wall due to the low stretching of the polymer sheet in this region. However, the large plastic deformation of the polymer sheet on the mold's wall leads to a significant increase of the temperature. Figure 11 show that more the polymer becomes soft more the adiabatic heating is less important. This behavior is accounted for by introducing the temperature dependence of the physical properties ($\rho(\theta)$ and $c(\theta)$) in the eq. (15), which is given by eqs. (19) and (20).

CONCLUSION

We have successfully implemented a micromechanical model for the simulation of the thermoforming process of the amorphous thermoplastic polymers. The behavior of the polymeric material is described by a temperature and strain rate sensitive elastic viscoplastic model. The simulations are conducted using the finite element method. The predicted results show a strong dependence of the polymeric sheet thickness and molecular orientation on the process temperature. The sheet thickness depends on the applied pressure and the contact forces, which rise once the sheet reaches the mold surface. The high stretching on the mold's wall leads to high orientation of the polymer molecular chains, which in turn results in high mechanical properties of the final product at this region.

References

1. Argon, A. S. Philos Mag 1973, 28, 839.
2. Aus Der Wiesche, S. Appl Therm Eng 2004, 24, 2391.
3. Warby, M. K.; Whiteman, J. R.; Jiang, W. G.; Warwick, P.; Wright, T. Math Comput Simulat 2003, 61, 209.
4. Schmidt, F. M.; Le Maoult, Y.; Monteix, S. J Mater Process Technol 2003, 225, 143.
5. Abaqus/explicit manuals version 6.5, Abaqus Inc.; Rising Mills, 166 Valley Street, Providence, RI 02909, USA.
6. Boyce, M. C.; Socrate, S.; Llana, P. G. Polymer 2000, 41, 2183.
7. Makradi, A.; Ahzi, S.; Gregory, R. V.; Edie, D. D. Int J Plast 2005, 21, 741.
8. Ahzi, S.; Makradi, A.; Gregory, R. V.; Edie, D. D. Mech Mater 2003, 33, 1139.
9. Boyce, M. C.; Parks, D. M.; Argon, A. S. Mech Mater 1988, 7, 15.
10. Richeton, J.; Ahzi, S.; Vecchio, K. S. J Mech Phys Solids, to appear.
11. Sarva, S.; Mulliken, A. D.; Boyce, M. C. Int J Solids Struct 2007, 44, 2381.
12. Arruda, E. M.; Boyce, M. C. J Mech Phys Solids 1993, 41, 931.
13. William, M. L.; Landel, R. F.; Ferry, J. D. J Am Chem Soc 1955, 77, 3701.
14. Bergstrom, J. S.; Boyce, M. C. J Mech Phys Solids 1998, 46, 931.
15. Doi, M.; Edwards, M. F. The Theory of Polymer Dynamics; Oxford University Press: Oxford, 1986.
16. Arruda, E. M.; Boyce, M. C.; Jayachandran, R. Mech Mater 1995, 19, 193.
17. Boyce, M. C.; Montagut, E. L.; Argon, A. S. Polym Eng Sci 1992, 32, 1073.
18. Doolong, P. J.; Buckley, C. P.; Rostami, S.; Zahlan, N. Polymer 2002, 43, 2451.
19. van Krevelen, D. W. Properties of Polymers, 3rd ed.; Elsevier: Amsterdam, 1990.
20. Bicerano, J. Prediction of Polymer Properties; Marcel Dekker: New York, 1993.
21. Dong, Y.; Lin, R. J. T.; Bhattacharyya, D. J. Mater Sci 2005, 40, 399.
22. Dong, Y.; Lin, R. J. T.; Bhattacharyya, D. Polym Polym Compos 2006, 14, 307.